Talanta 82 (2010) 876–884

Contents lists available at ScienceDirect

Talanta

journal homepage: www.elsevier.com/locate/talanta

Titania nanowires as substrates for sensing and photocatalysis of common textile industry effluents

Soumit S. Mandal, Aninda J. Bhattacharyya*

Solid State and Structural Chemistry Unit, Indian Institute of Science, Malleshwaram, Bangalore 560012, Karnataka, India

ARTICLE INFO

Article history:
Received 10 February 2010
Received in revised form 11 April 2010
Accepted 12 April 2010

Keywords:
Titana nanowires
Water pollution
Textile dyes
Electrochemical sensing
Photocatalysis

ABSTRACT

Sensing and photocatalysis of textile industry effluents such as dyes using mesoporous anatase titania nanowires are discussed here. Spectroscopic investigations show that the titania nanowires preferentially sense cationic (e.g. Methylene Blue, Rhodamine B) over anionic (e.g. Orange G, Remazol Brilliant Blue R) dyes. The adsorbed dye concentration on titania nanowires increased with increase in nanowire dimensions and dye solution pH. Electrochemical sensing directly corroborated spectroscopic findings. Electrochemical detection sensitivity for Methylene Blue increased by more than two times in magnitude with tripling of nanowire average length. Photodegradation of Methylene Blue using titania nanowires is also more efficient than the commercial P25-TiO_2 nanopowders. Keeping illumination protocol and observation times constant, the Methylene Blue concentration in solution decreased by only 50% in case of P25-TiO_2 nanoparticles compared to a 100% decrease for titania nanowires. Photodegradation was also found to be function of exposure times and dye solution pH. Excellent sensing ability and photocatalytic activity of the titania nanowires is attributed to increased effective reaction area of the controlled nanostructured morphology.

1. Introduction

Among various semiconducting oxides, unique physical and chemical properties make titania (TiO_2) exceptionally attractive for a wide range of applications such as catalysis, electrochemical energy storage, and photovoltaics [1]. Extensive efforts have been made to further enhance performance and range of applications of TiO_2. Research has been predominantly concentrated on development of improved materials via optimized synthesis methods. Some of the key approaches towards synthesis of improved TiO_2 materials have been reduction in size ($\mu m \rightarrow nm$) and dimensions (three (e.g. sphere) $\rightarrow$ zero (e.g. quantum dots)), designing of various architectures at reduced length scales (nanometer), compositional manipulations (e.g. TiO_2 composites). Examples of such endeavors have already been demonstrated in various fields especially with regard to photocatalysis [2–7], electrochemical energy storage and generation (rechargeable lithium-ion batteries [8–10], solar cells [11,12]), biotechnology (drug delivery, biosensing [13–17], chemosensing [18]) and catalysis [19]. Intrinsic materials properties which have been observed to determine material's function in various applications are crystallographic structure, morphology (size and shape) and surface chemistry. TiO_2 has also been demonstrated to be bio-friendly as immobilization of biomolecules such as proteins did not lead to any detrimental effects on the native structure and function. With regard to enzymes, it has been observed that immobilization inside TiO_2 enhances enzymatic activity leading to potential biosensor applications [13,14].

Recently, ecology related problems associated with water pollution have attracted a lot of attention and it is envisaged that nanostructured semiconducting oxide materials can play a major role in this respect too. There are various sources of water pollution the major ones being radioactive waste [20,21], sewage and wastewater, underground storage leakages and industrial waste [22–27]. Release of toxic chemical waste such as pesticides, fertilizers, and dyes comprises a major source of industrial water pollution. Detection and removal of these toxic chemicals are a major challenge. There have been reports discussing detection of various metal ions in solutions using various techniques [28–30]. One of the major sources of water contamination has been identified to originate from the textile industries where approximately 15% of the dyes used during synthesis and processing are released as waste in to ground or river water. These dyes not only affect aesthetic merit of water but also reduce light penetration and photosynthesis, and some have been designated as carcinogenic to humans. Thus there is an urgent need of environmental-friendly technologies for the detection and removal of textile effluents from water. It has been shown that dyes can be easily adsorbed and catalyzed on oxide surfaces. The catalysis reaction depends among

* Corresponding author. Tel.: +91 80 22932616; fax: +91 80 23601310.
E-mail addresses: aninda_jb@sscu.iisc.ernet.in, aninda_jb@yahoo.com (A.J. Bhattacharyya).

0039-9140/$ – see front matter © 2010 Elsevier B.V. All rights reserved.
doi:10.1016/j.talanta.2010.04.021

several factors the effective surface area of interaction between the dye solution and the oxide. In this context, it would be beneficial to employ nanostructured materials as this allows higher interaction area resulting in higher adsorption yield on the oxide surface. Most of the work in published literature [31–34] using semiconducting nanometer sized oxide materials such as TiO_2 employ the process of photodegradation to remove and quantify dyes in solution. To our knowledge there exists only a few reports [35] which aim at direct removal/sensing of the common industrial dyes via electrochemical methods. We present here a detailed study of electrochemical and spectroscopic detection (and quantification) of various commonly used textile dyes e.g. cationic—Methylene Blue, Rhodamine B and anionic—Orange G, Remazol Brilliant Blue R in aqueous solution using TiO_2 nanowires. In addition, we also discuss the photocatalytic degradation using TiO_2 nanowires as a function of various parameters. In the subsequent sections we discuss the preparation, structural characterization, spectroscopic and electrochemical detection and photocatalysis of various industrial dyes.

2. Materials and methods

2.1. Starting materials and synthesis of titania nanowires

Titanium (IV) tetraisopropoxide (TTIP, Sigma), Methylene Blue (MB), Orange G (OG), Rhodamine B (RB) (all dyes from S.D. Fine Chemicals Ltd., India) and Remazol Brilliant Blue R (RBBR, Colour Chem. Ltd., India) were used as received. Ethylene glycol (EG, S.D. Fine Chemicals) employed for the preparation was distilled and stored under inert nitrogen atmosphere until further use. In a typical synthesis [36], titanium glycolate nanowires having uniform diameter are synthesized first. 0.050 ml (~0.147 mmol) TTIP was added to 50 ml of EG under nitrogen gas flow in a sealed glove bag (Sigma). The solution was then taken out of the glove bag and heated to 170 °C for 2 h under constant stirring. Following cooling down to room temperature, the white flocculate was separated via centrifugation and then washed with deionised water and ethanol several times for complete removal of excess EG from the sample. Dry titanium glycolate nanowires were obtained by heating the precipitate under vacuum at 50 °C for 4 h. Calcination of the glycolate nanowires at 500 °C for 3 h in a muffle furnace resulted in the formation of titania (TiO_2) nanowires.

2.2. Characterization for probing TiO_2 nanowire morphology, structure and adsorption ability of various dyes

General morphology, structure of the nanowires and the extent of dye adsorption on the nanowires were performed using transmission/scanning electron microscopy, powder X-ray diffraction (XRD), Fourier transform infrared spectroscopy (FTIR), thermogravimetry analysis (TGA) and N_2 adsorption/desorption isotherms. Transmission electron microscope (TEM) images were observed and recorded (FEI Tecnai F30) with an acceleration voltage of 200 kV. 2 μl of TiO_2–ethanol solution was dropped on a Cu grid with a carbon-reinforced plastic film. Scanning electron microscopy was done (FEI SIRION) in the voltage range of 200–300 kV. For FTIR and XRD analysis, approximately 55–60 mg of titania was soaked in 100 ml of 50 ppm dye solution for approximately 4 h. The titania nanowires coated with the dye (abbreviated as D-TiO_2, D = MB, OG) was separated out from the solution via centrifugation and dried at 50 °C (dye melting point ≈ 100 °C) under vacuum. X-ray diffraction patterns (X'pert Pro Diffractometer, Phillips, Cu K_α radiation) were recorded in the 2θ range from 5° to 65° at a scanning rate of 1° min^{-1}. For room temperature (=25 °C) FTIR measurements (FTIR Spectrometer spectrum 1000, PerkinElmer), requisite amount of D-TiO_2 was mixed with pure spectroscopic grade potassium bromide (KBr) and cast into a pellet of diameter 1.3 cm and thickness ~0.1 cm. Thermogravimetry analysis (TGA, PerkinElmer Pyris6000) experiments were done by heating the sample in a silica crucible from 30 to 700 °C at a heating rate of 10 °C min^{-1} in N_2 atmosphere. For N_2 adsorption/desorption (Belsorp-Max) experiments titania nanowires were degassed at 150 °C for 5 h whereas the dye–titania composites were degassed at 25 °C (dye decomposition temperatures ~100 °C) for 2 h. The dye adsorption kinetics were studied using UV–vis absorption spectroscopy (PerkinElmer, Lambda 35 UV Spectrometer, path length = 1 cm). 0.1 g of titania (nanowires) was added to 100 ml (of 50 ppm, say) dye solution and stirred continuously for 2 h for homogeneity. Aliquots were collected from the reaction beaker at different time intervals and concentration of dye in solution as a function of time was determined by monitoring the changes in the λ_{max} line intensity with time.

2.3. Electrochemical measurements for sensing dye content in aqueous solution: preparation of modified electrode

The glassy carbon electrode was coated with the TiO_2 nanowire using a standard droplet evaporation procedure described in ref [37–40]. Firstly, titania–water solution (10 mg of titania per ml of water) was prepared and vortexed adequately. Glassy carbon electrode (GCE, diameter: 3 mm) was polished with 0.3 μm alumina slurry to a mirror finish. After each polishing step the electrode was rinsed and ultrasonicated respectively in ethanol and redistilled water for 60 s. 20 μl of aqueous titania solution was dropped on the shining surface of GCE and dried for 3–4 h in air at room temperature (25 °C). The uniformity in the TiO_2 film thickness could not be precisely controlled due to the liquid evaporation. The thickness of the film was approximately estimated to be 5 μm and photographic visualization (not shown here) showed that the TiO_2 coverage remained same before and after the cyclic voltammetry experiments. Further, evidence with regard to the uniformity of the TiO_2 films can be seen from the sensing experiments using cyclic voltammetry. This will be discussed in detail in a subsequent section.

2.4. Cyclic voltammetry for dye detection

The electrochemical response of the dye in solution was estimated using cyclic voltammetry (CH608C, CH Instruments). The working, counter and reference electrodes were TiO_2/GCE, platinum wire and saturated calomel electrode respectively. The electrodes were dipped in 5 ml of dye-deionised water solution having varying dye concentrations (approximately 15–100 ppm). The solution was deoxygenated for 30 min prior to the start of the measurements and nitrogen atmosphere was maintained throughout the duration of the experiment.

2.5. Photocatalytic degradation of dyes in aqueous solution

The photochemical reactor used in this study was made of a Pyrex glass jacketed quartz tube. A high pressure mercury vapor lamp (HPML) of 125 W (Philips, India) was placed inside the jacketed quartz tube. To avoid fluctuations in the input light intensity, supply ballast and capacitor were connected in series with the lamp. Water was circulated through the annulus of the quartz tube to avoid heating of the solution. 100 ml of the solution was taken in the outer reactor and continuously stirred to ensure that the suspension of the catalyst was uniform. The lamp radiated predominantly at 365 nm corresponding to energy of 3.4 eV and photon flux of 5.8×10^{-6} mol of photons/s. For the photocatalysis experiments with TiO_2 nanowires, three concentrations of MB dye (20 ppm, 30 ppm and 50 ppm, all in 100 ml) were used (0.1 g of TiO_2

in 100 ml of dye solution). Photocatalysis experiments were also done with adequate amounts of commercial P25-TiO_2 (Degussa, BET surface area = 50 m^2 g^{-1}) powder dispersed in 50 ppm of 100 ml solution.

3. Results and discussion

3.1. Titania nanowire morphology via electron microscopy

Fig. 1 shows the SEM (a) and TEM (c) images of titania nanowires obtained from intermediate titanium glycolate nanowires via the synthesis procedure described in the experimental section (morphology of the intermediate titanium glycolate were almost the same as final titania nanowires, cf. supporting information). The approximate average length and diameter of the nanowires were respectively 3 μm (2–4 μm as per frequency distribution plot, Fig. 1b) and 800 nm. The nanowire dimensions were also observed to be dependent on preparation conditions. Heating of the TTIP-EG mixture for longer hours resulted in longer wires. Fig. 1e shows the SEM image of titania nanowires resulting out of heating the TTIP-EG mixture for 6 h (instead of 2 h; cf. Section 2) at 170 °C keeping the calcination temperature (=500 °C) and time (=3 h) same. While the average length increased from approximately 3 μm to 20 μm,

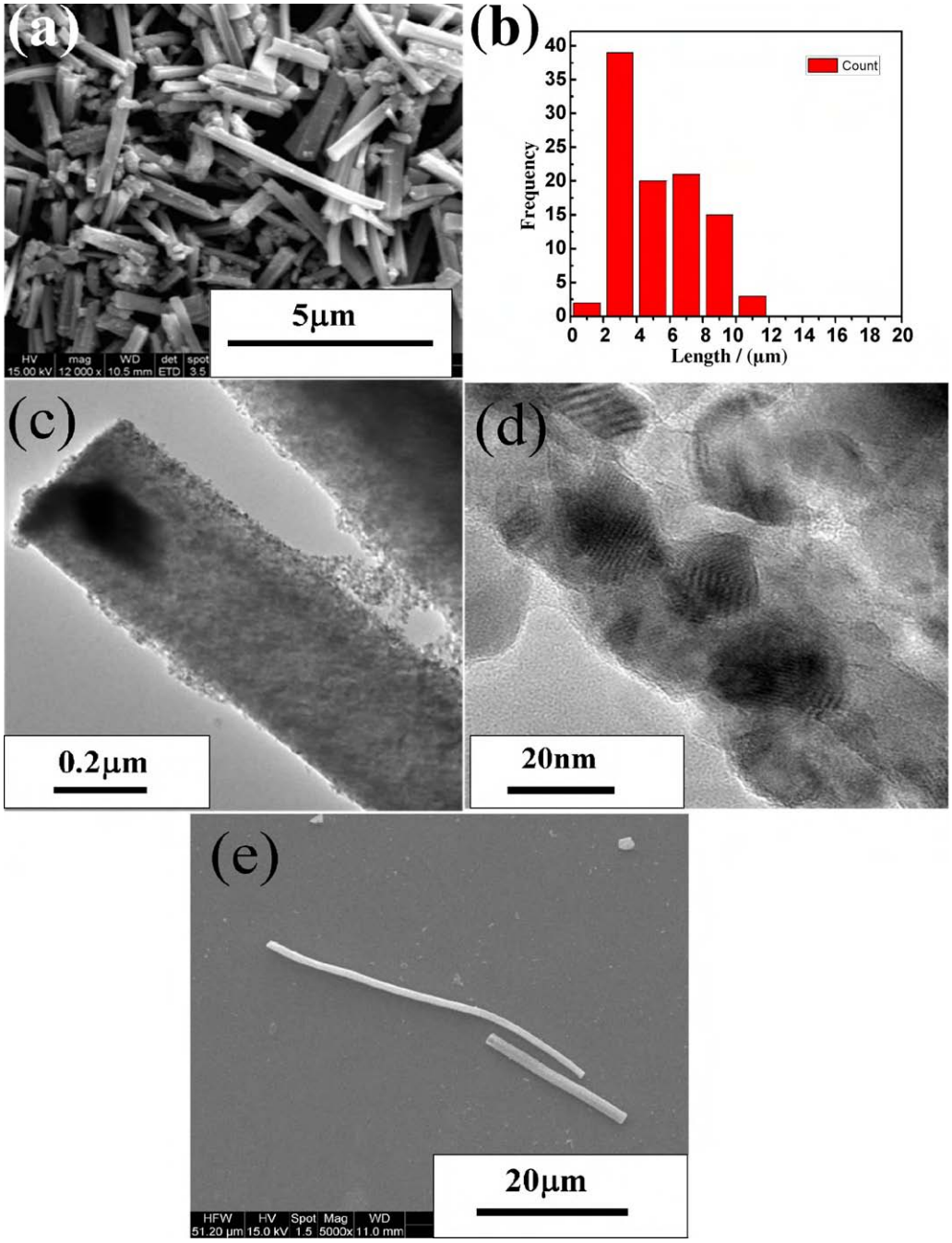

Fig. 1. (a) Scanning electron micrograph of TiO_2 nanowires; (b) length distribution of TiO_2 nanowires; (c) transmission electron micrographs showing the solid wire-like morphology; (d) high resolution transmission electron micrographs of the TiO_2 nanowires showing certain degree of surface porosity. (a–d) Sample preparation conditions: reaction time 2 h at 170 °C; calcination temperature = 500 °C. (e) Scanning electron micrographs of the longer TiO_2 nanowires (reaction time = 6 h at 170 °C; calcination temperature = 500 °C).

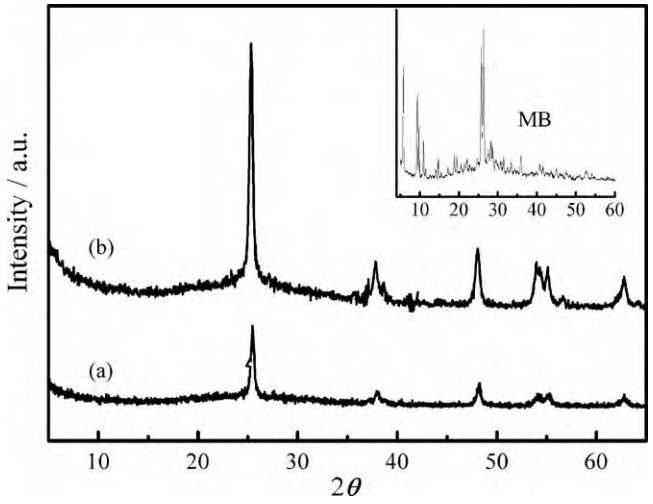

Fig. 2. Room temperature X-ray diffraction (XRD) pattern showing the anatase phase of TiO_2. (a) Bare TiO_2; (b) MB–TiO_2. Inset: X-ray diffraction pattern of MB in solution (MB: Methylene Blue).

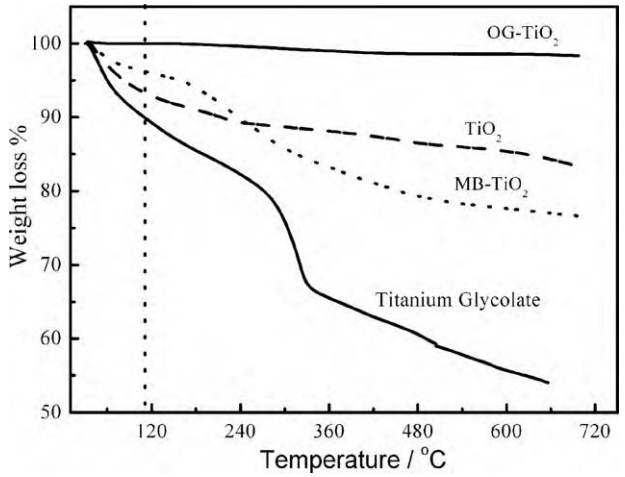

Fig. 3. Thermogravimetry analysis (TGA) of various samples (temperature range: 30–700 °C, heating rate: 10 °C min^{-1} under nitrogen flow). TiO_2 nanowire dimensions: length: 3 μm and diameter = 0.8 μm.

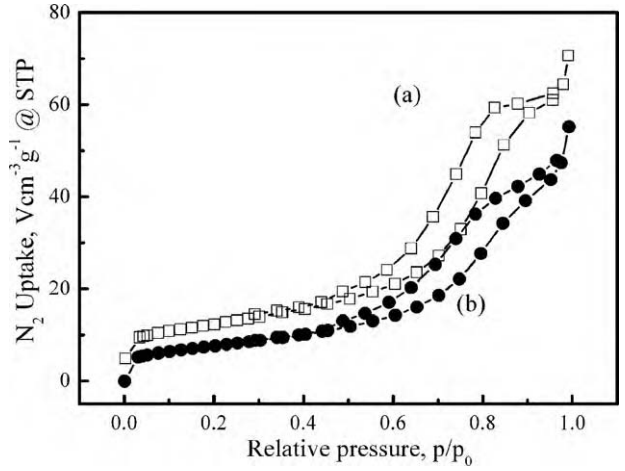

Fig. 4. N_2 adsorption/desorption isotherms of various samples: (a) TiO_2; (b) MB-TiO_2. All samples were degassed at appropriate temperatures prior to the measurements.

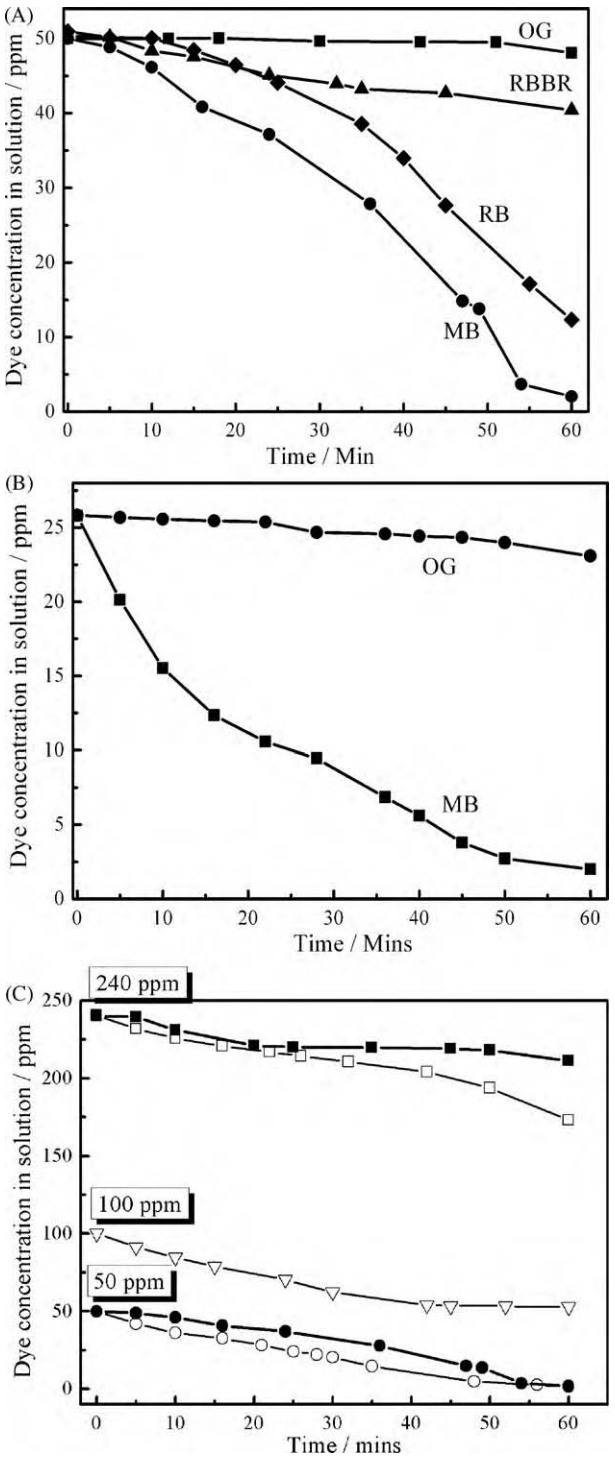

Fig. 5. Variation in solution dye concentration with time as a result TiO_2 nanowires (dimensions: length: 3 μm and diameter = 0.8 μm) dispersion in (A) various dye solutions. (B) A solution mixture of Methylene Blue (MB) and Orange G (OG). (C) A solution having different initial MB concentrations: (a) 50 ppm, (b) 100 ppm, and (c) 240 ppm. Filled symbols for shorter TiO_2 nanowires: length: 3 μm and diameter = 0.8 μm; unfilled symbols for longer TiO_2 nanowires: length: 20 μm and diameter = 1.5 μm.

the diameter became approximately double. The wires appeared to be porous as observed from high resolution TEM images (Fig. 1d). We propose the source of porosity to the existence of pores in between the TiO_2 particle aggregates which leads to the formation of nanowire morphology. Porosity and nature of pore arrangement will be further discussed in the context of N_2 adsorption/desorption isotherms in a subsequent section.

3.2. X-ray diffraction to study titania structure and detection of dye adsorption

The X-ray diffraction pattern of the synthesized TiO_2 nanowires (Fig. 2a) could be completely indexed to anatase phase (JCPDS file no. 21-1272). The crystallite size (d) estimated from the full width at half maximum (w) of the dominant (1 0 1) peak at diffraction angle $2\theta \approx 25.2^\circ$ using Scherrer's equation was found to be 19 nm. This is also confirmed by high resolution TEM images (Fig. 1d). The X-ray diffraction pattern of the nanowires loaded with MB dye (Fig. 2b) was found to be very similar to the bare nanowires (Fig. 2a). However, the peaks for dye–nanowires appeared to have sharper contours and were more intense compared to the unloaded ones (significant number of peaks of pure MB appears almost at the same position as pure TiO_2, Fig. 2 inset). The TiO_2 surface may induce nucleation of adsorbed MB dye leading to crystallization on the oxide surface. This accounts for the observed changes in diffraction pattern between bare TiO_2 to dye–TiO_2 nanowires.

3.3. Thermogravimetry analysis for estimation of dye uptake on TiO_2 nanowires

The compositional changes of various samples were investigated using TGA. Fig. 3 exhibits a two-step weight loss when titanium glycolate samples were heated under nitrogen flow between 30 and 700 °C under nitrogen gas flow. While the first step weight loss is attributed to the desorption of physisorbed water and ethylene glycol, the second step is ascribed to decomposition of ethylene glycol units and degradation of organic groups comprising the glycolate nanowires [41]. The combined (first step + the second step) weight loss (calculated from 110 °C) in case of titanium glycolate nanowires was 22%. The thermogravimetry trace of the TiO_2 nanowires obtained from calcination of titanium glycolate showed only an initial weight loss (~10%) corresponding mainly to the physisorbed water and some residual organic impurities. No additional weight loss similar to that of titanium glycolate was observed. This strongly suggests that the chosen calcination temperature is able to completely convert the titanium glycolate to TiO_2. The MB–TiO_2 showed a weight loss of approximately of 25% in the temperature regime 110–700 °C which is attributed to both water and MB dye decomposition. The OG–TiO_2 showed negligible weight loss (~2%) in the similar temperature regime. The higher percentage weight loss in case of MB compared to OG suggests that TiO_2 nanowires preferentially adsorb cationic dyes (such as MB) than anionic dyes (such as OG). This point will be further exemplified via other characterization procedures in the subsequent section.

3.4. N_2 adsorption/desorption studies

As discussed in the context of TEM studies, N_2 adsorption/desorption were performed to assess the porosity as well as morphology of pores (Fig. 4). Additionally, N_2 adsorption/desorption were also performed to judge the extent of dye adsorption on the TiO_2 nanowires. The isotherm obtained for the bare as well as dye loaded nanowires can be classified to type IV. Significant degree of hysteresis was also observed between the adsorption and desorption isotherms. The nature of the isotherms strongly suggests presence of mesoporosity in the anatase TiO_2 nanowires. The BET surface area for bare titania nanowires was estimated to be approximately 43 $m^2\,g^{-1}$ and following MB adsorption on nanowires the surface area decreased to 24 $m^2\,g^{-1}$ (isotherm for MB–TiO_2 corresponds to initial dye concentration of 50 ppm in 100 ml solution for 0.1 g of 3 μm long TiO_2 nanowires).

3.5. Adsorption of dye on TiO_2 surface via UV–vis spectroscopy

The λ_{max} values for OG and MB appear at 450 nm and 664 nm respectively and their intensities vary differently with time following introduction of TiO_2 nanowires in respective dye solutions (Fig. 5A). While the color intensity of the MB–TiO_2 solution decreased progressively over a period of approximately 60 min (t_0 = 50 ppm; t_{60} = 2 ppm), color of OG-TiO_2 solution remained almost unaltered in the same period of time (t_0 = 50 ppm;

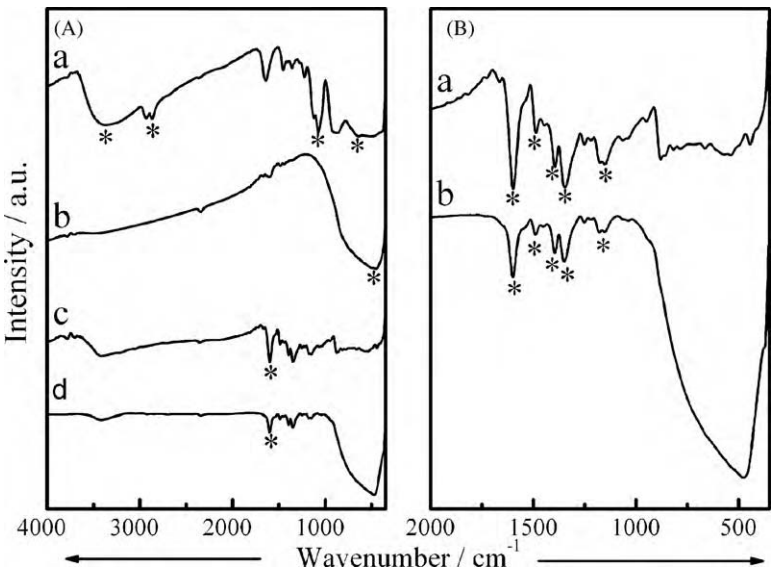

Fig. 6. Fourier transform infrared spectra (FTIR) at 25 °C for various samples. (A) Spectral range: 4000–350 cm^{-1}: (a) titanium glycolate nanowires, (b) bare TiO_2, (c) MB in solution, and (d) MB–TiO_2. (B) Spectral range 2000–350 cm^{-1}: (a) MB in solution and (b) MB–TiO_2 (MB: Methylene Blue). TiO_2 nanowire dimensions: length: 3 μm and diameter = 0.8 μm. The symbol "*" represents the important IR bands.

t_{60} = 48 ppm). Beyond 60 min till 120 min (not shown here) no further decrease in λ_{max} line intensity i.e. no color change takes place. From observation of time variation of λ_{max} intensity, we propose that the TiO_2 nanowires preferentially adsorb cationic MB dye compared to anionic OG dye. This also supports similar conclusions from TGA where higher weight loss was observed in case of the MB–TiO_2 compared to OG–TiO_2. To further validate the preference of the nanowires for cationic dyes, λ_{max} line intensity variation with time was carried out using a different cationic (Rhodamine B (RB), λ_{max} = 554 nm) and an anionic dye (Remazol Brilliant Blue R (RBBR), λ_{max} = 591 nm). Results with respect to RB and RBBR were similar to as obtained for MB and OG. In another experiment TiO_2 nanowires were dispersed in a solution mixture of MB and OG (1:1 by w/w). The intensity of λ_{max} line (at 664 nm) for MB decreased progressively as a function of time (≡TiO_2 in a solution containing MB alone) while λ_{max} band for OG changed only negligibly (≡TiO_2 in a solution containing OG alone) in the same period of time (Fig. 5B). These experiments again convincingly demonstrate that TiO_2 nanowires have a preference for cationic dyes. The preference for cationic dyes is attributed to the negative charge on TiO_2 nanowire surface. Presence of negative charge on the titania nanowire surface was confirmed via preliminary electrophoretic ζ-potential (Zetasizer Nano ZS, Malvern Instruments) measurements of TiO_2 nanowires in deionised water which yielded a negative potential of approximately −46 mV.

Fig. 5C shows λ_{max} line intensity variation as a function of time for various MB concentrations in solution (TiO_2 concentration kept constant for all dye concentrations per 100 ml dye solution). The extent of dye adsorption on titania surface is observed to depend on the initial dye concentration in solution as well as on titania nanowire size. For TiO_2 nanowires of a particular size (say, length: 3 μm and diameter = 800 nm), total amount of adsorbed dye on nanowire surface in a fixed span of time (=60 min) deceased with increase in initial solution dye concentration. This implies that the amount of MB remaining in solution increased with increase in initial dye concentration. The observed trend in variation of adsorbed dye concentration on nanowire as a function of initial solution dye concentration is attributed to the existence of a saturation limit which essentially corresponds to the dye concentration resulting in full coverage of the TiO_2 surface. Once the surface of nanowires is fully covered with a monolayer of dye molecules, additional dye molecules diffusing towards the TiO_2 nanowire surface will be repelled back electrostatically thus preventing further dye adsorption on the oxide surface. With increase in TiO_2 nanowire dimensions the saturation dye concentration is expected to shift to higher concentrations. This is clearly evident from Fig. 5C. Higher concentrations of dye are adsorbed (higher decrease in solution dye concentration) on the larger nanowires (length: 20 μm and diameter = 1.5 μm) even at very high initial concentration of dye in solution (such as 240 ppm).

3.6. Fourier transform infrared (FTIR) spectroscopy

Fig. 6A and B shows the FTIR spectra of bare TiO_2 and MB–TiO_2. FTIR observations obtained here are in line with previous reports describing synthesis of various phases of titania using conventional alkoxides as sol–gel precursors [42]. The peaks corresponding to the physically adsorbed water or ethylene glycol (O–H stretching mode at ∼3400 cm^{-1} and O–H bending mode at ∼1640 cm^{-1}) observed in case of nanowires following directly from the polyol synthesis disappeared completely on calcining at 500 °C (Fig. 6A(a, b)). The band at 453 cm^{-1} is attributed to the Ti–O stretching band. The IR spectrum of MB and MB–TiO_2 are shown in (Fig. 6A(c, d) and B (a, b)). Bands at 1598 cm^{-1}, 1486 cm^{-1}, 1394 cm^{-1}, 1345 cm^{-1}, 1251 cm^{-1}, 1150 cm^{-1} respectively correspond to C=N, C=C, multiple ring stretching, $C_{aromatic}$–N, N–CH_3 of MB. Similar bands but

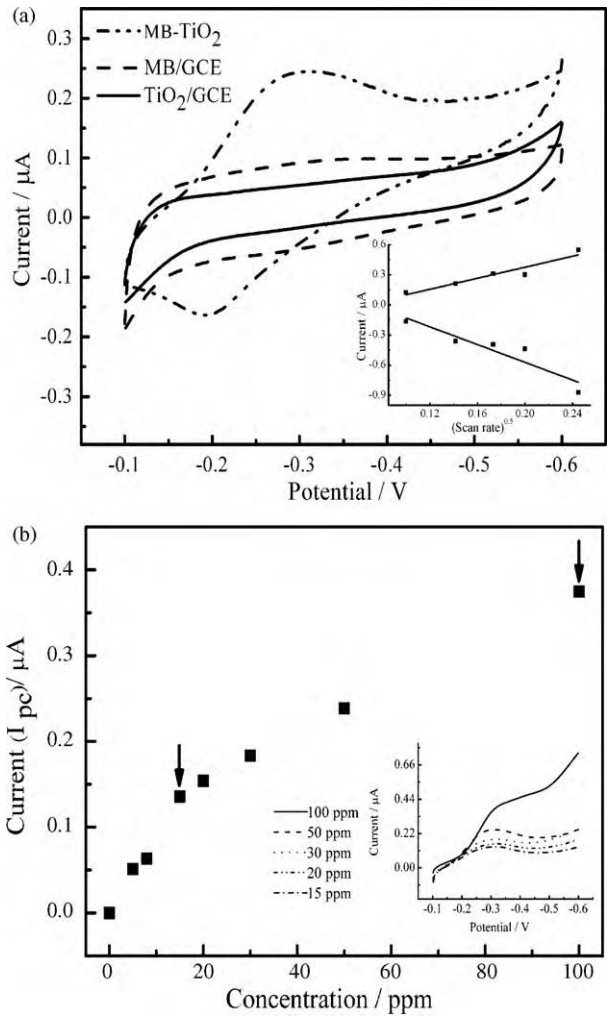

Fig. 7. (a) Cyclic voltammograms at 25 °C (scan rate of 0.01 V s^{-1}) for TiO_2/GCE (in water) MB/GCE and TiO_2/GCE (in 50 ppm MB in 100 ml solution). Inset: Shows the variation of I_{pc} and I_{pa} versus square root of scan rates ($v^{1/2}$) (MB: Methylene Blue). TiO_2 nanowire dimensions: length: 3 μm and diameter = 0.8 μm. (b) Variation of anodic current (from cyclic voltammetry at 25 °C at scan rate 0.01 V s^{-1}) with different initial Methylene Blue (MB) concentrations (0–100 ppm) in 100 ml solution. Inset: Cyclic voltammogram of MB–TiO_2 with different MB concentrations (0–100 ppm). TiO_2 nanowire dimensions kept same.

with reduced intensities were also observed for the MB–TiO_2 sample. This assures that the residence of MB dye molecules on the TiO_2 surface and also implying the utility of TiO_2 nanowires as substrates in specific detection and quantification of certain class of dyes in solution. OG–TiO_2 sample did not exhibit (not shown here) any characteristic OG band of appreciable intensities. This suggests the presence of negligible OG amounts on the TiO_2 surface and also further exemplifies the specificity of the present titania nanowires towards certain class of dyes in solution only.

3.7. Electrochemical detection and quantification of Methylene Blue (MB) in solution using TiO_2 nanowires

Owing to the preferential adsorption of cationic dyes by the TiO_2 nanowires, we restrict our discussion on electrochemical detection and quantification to cationic dyes only. We have chosen Methylene Blue as the representative cationic dye for sensing as well as for photocatalysis studies (discussed in detail in a subsequent section). Fig. 7a shows the electrochemical responses of various working electrodes: MB/GCE (i.e. GCE dipped in aqueous MB solution),

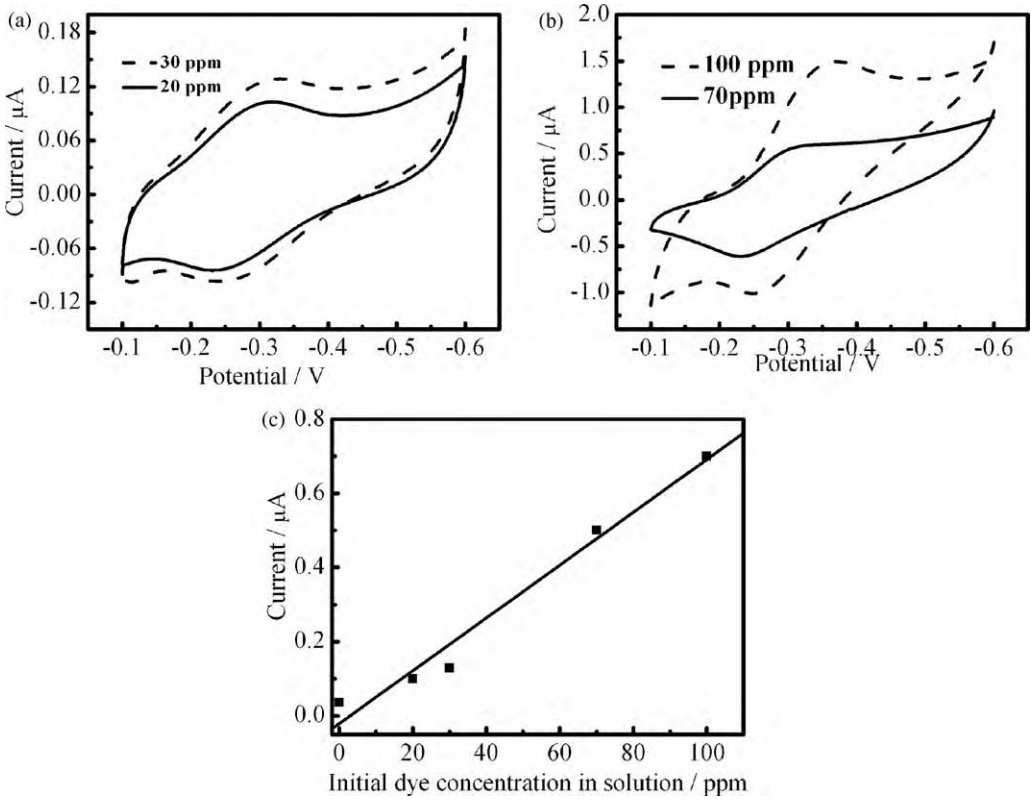

Fig. 8. (a and b) Cyclic voltammograms at 25 °C (scan rate of 0.01 V s^{-1}) for TiO_2/GCE (in deionised water) MB/GCE and TiO_2/GCE (in different initial Methylene Blue (MB) concentrations (0–100 ppm) in 100 ml solution). (c) Variation of anodic current with different initial Methylene Blue (MB) concentrations (0–100 ppm) in 100 ml solution. TiO_2 nanowire dimensions: length: 20 μm and diameter = 1.5 μm.

TiO_2 (length: 3 μm and diameter = 0.8 μm)/GCE in pure deionised water and in different concentration of aqueous MB solutions. The absence of redox peaks in case of TiO_2 (length: 3 μm and diameter = 0.8 μm)/GCE (in deionised water) suggests electroinactivity of the system in the applied potential window. The GCE electrode in MB solution showed very broad (and low current intensity) reversible peaks at approximately −0.36 V and −0.29 V. The TiO_2 (length: 3 μm and diameter = 0.8 μm)/GCE electrode assembled in aqueous MB solution (50 ppm) also showed a pair of well defined reversible peaks at −0.31 V and −0.19 V however, the redox peak currents were much higher in magnitude compared to MB/GCE (50 ppm) and TiO_2 (length: 3 μm and diameter = 0.8 μm)/GCE electrode assemblies (in deionised water). This is in stark contrast to the response of the bare GCE in 50 ppm of MB solution (Fig. 7a) where only broad peaks were obtained. The enhanced current response such as that observed for the TiO_2/GCE (≈50 ppm MB solution) electrode, with the bare GCE can be observed only at a very high concentration of the MB dye (≈150 ppm). So the presence of TiO_2 nanowires on GCE enhances the yield of the MB redox reaction and thus amicably demonstrates TiO_2 nanowires as suitable sensor. Additionally, the TiO_2 film was very stable before and after the cyclic voltammetry experiments. Negligible current changes were observed from one cycle to another during the cyclic voltammetry measurements. This rules out any detrimental morphological changes in the TiO_2 film including issues such as lixiviation. This is evident from the negligible changes in current values from cycle to another during cyclic voltammetry. The electrode reaction of MB involves two successive one-electron charge transfer coupled with a rapid reversible protonation between MB^+ and leucomethylene blue (LMB) [43,44]. Fig. 7a (inset) shows the linear increase in redox peak current with increasing scan rates for the TiO_2 (length: 3 μm and diameter = 0.8 μm)/GCE electrode assembly in MB solution. The linear variation indicates that the redox reaction of MB at TiO_2 (length: 3 μm and diameter = 0.8 μm)/GCE electrode is a diffusion-controlled process. The surface active concentration of MB attached to the TiO_2 surface obtained from the integration of the reduction peak was found to be 6.5×10^{-11} mol cm^{-2}.

Fig. 7B shows the cyclic voltammograms of TiO_2 (length: 3 μm and diameter = 0.8 μm)/GCE electrode system in aqueous solutions with different initial concentrations of MB (15–100 ppm). This study was performed to estimate the sensitivity of the TiO_2 nanowires for possible use as substrates in sensors for detection of cationic industrial dyes. The cathodic current corresponding to the peak at −0.31 V increased linearly with increasing initial concentration of MB in solution. From the slope of the linear fit (i_{pc} (μA) = 0.09835 + 0.00277 [MB]/ppm) to current versus initial solution dye concentration data (Fig. 7b) the sensitivity was estimated to be approximately 0.003 μA ppm^{-1}. Due to the dependence on degree of dye coverage on TiO_2 nanowire dimensions, the sensitivity too was observed to be dependent on the TiO_2 nanowire dimensions. Fig. 8a and b shows cyclic voltammograms with longer TiO_2 (length: 20 μm and diameter = 1.5 μm)/GCE electrode system in aqueous solutions with different initial concentrations of MB (20–100 ppm). Similar to the shorter wires, the cathodic current corresponding to the cathodic peak potential located at −0.31 V also increased with increasing concentration of MB (the magnitude of cathodic currents in case of the longer nanowires were much higher compared to the shorter ones). From the slope of the linear fit (i_{pc} (μA) = 0.03485 + 0.00713 [MB]/ppm) to current versus initial dye concentration in solution data (Fig. 8c) the sensitivity was estimated to be approximately 0.007 μA ppm^{-1}. Thus, sensing capabilities are enhanced with increase in size of TiO_2 nanowires.

3.8. Photocatalytic degradation of Methylene Blue (MB) by TiO_2 nanowires

The MB–TiO_2 nanowire solution mixture (0.1 g of TiO_2 nanowire in 20 ppm/30 ppm/50 ppm in 100 ml solution) was repeatedly illuminated for 5 min at 2 min intervals. During the 2 min interval, 1 ml aliquots were obtained from the test mixture. Due to progressive degradation of the dye with consecutive flashes the color of the solution mixture (as well as aliquots) changed from blue to light blue to finally white. The change in dye solution color or dye degradation as a function of time was monitored using UV–vis spectroscopy. For all initial solution MB concentrations (20–50 ppm), λ_{max} line intensity decreased with varying rates to negligibly small values over a period of 60 min. This suggests that TiO_2 nanowires are highly efficient substrates for degradation of azo-dyes such as Methylene Blue (MB). We also propose that the rate of dye degradation can be fine tuned via controlled variation of the nanowire dimensions i.e. larger the nanowires faster will be the rate of degradation. The catalytic performance of the TiO_2 nanowires was compared with commercial P25-TiO_2 nanoparticles. The amount of P25-TiO_2 was ascertained following consideration of the differences in surface area between P25-TiO_2 (surface area = 50 $m^2\ g^{-1}$) and TiO_2 nanowires (surface area = 43 $m^2\ g^{-1}$). Illumination of dye–P25-TiO_2 solution mixture (0.08 g of P25-TiO_2 in 50 ppm of 100 ml solution) using the same flash protocol resulted in decrease in color intensity similar to that observed in case of TiO_2 nanowire. However, the final concentration of the dye in solution was much higher compared to that of TiO_2 nanowires. While in case of TiO_2 nanowires the concentration decreased by nearly 100% in 60 min, the concentration of dye in solution decreased to only 50% in the same time span in case of P25-TiO_2. The superior performance of the TiO_2 nanowires compared to the P25-TiO_2 powder is attributed to its beneficial microstructure. The mesoporosity of the TiO_2 nanowires also aids in enhancing the effective area of interaction. Lower dye degradation efficiency in case of P25-TiO_2 is probably due to aggregation of the spherical nanoparticles leading to loss of effective surface area of interaction. No such detrimental effects due to aggregation are expected to arise in case of the titania nanowires.

3.9. Photocatalytic degradation of Methylene Blue (MB) by TiO_2 nanowires at various pH and irradiation time

Fig. 9b and c shows the photocatalytic degradation of Methylene Blue as a function of pH and exposure times. The dye adsorption and degradation depend very heavily on the state of the surface and pH is one of the important parameters affecting the surface state [45–47]. Drastic changes were observed in the kinetics performed at various pH viz. pH = 4, 7, and 11 (corresponding photodegradation with P25-TiO_2 at different dye solution pH is shown in supporting information Fig. 4). The changes observed in the degradation studies are supplemented via UV–vis absorption studies shown in supporting information Fig. 2. While in alkaline solutions (pH = 11) MB degraded at a fast rate with the dye concentration decreasing to a very low value in ≈45 min, in acidic solutions (pH = 4) the rate became slower and degree of degradation was lower in the same time period. In alkaline solutions the TiO_2 (point of zero charge of TiO_2 (Degussa P25) is at pH = 6.8 [48]) surface becomes more negatively charged ($Ti–OH + OH^- \rightarrow TiO^- + H_2O$) resulting in higher dye adsorption and degradation of the dye. In acidic solutions TiO_2 surface becomes positively charged ($Ti–OH + H^+ \rightarrow TiOH_2^+$) resulting in lower adsorption and degradation of the dye. More appropriately, the differences in the dye adsorption and degradation at various pH under photo-irradiation can be understood in the manner demonstrated in ref [47]. At high pH, due to availability of copious amount of OH^-, the holes react with them to form radical OH ($OH^\bullet$) [49]. The $OH^\bullet$ reacts with the dye leading to degradation. Due to presence of less amount of $OH^\bullet$ at low pH, the degradation yield is mush lower. [47].

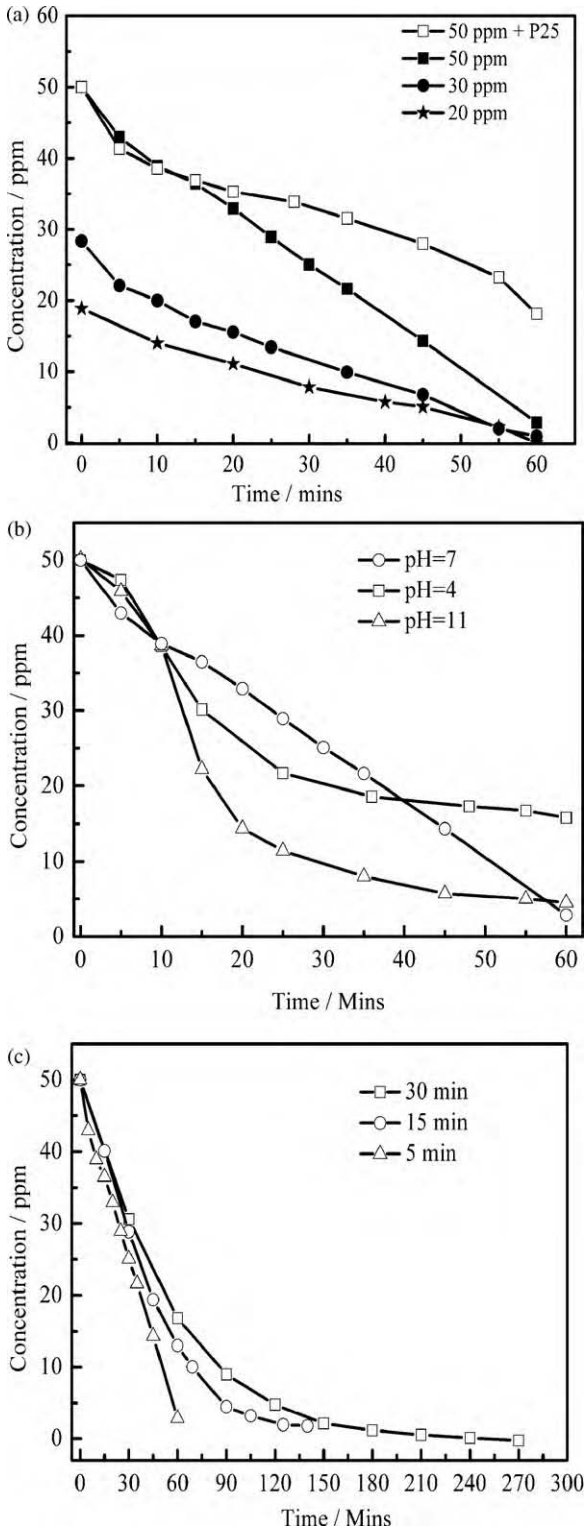

Fig. 9. Photocatalysis of Methylene Blue (a) 20–50 ppm of MB in 100 ml of solution using 0.1 g of TiO_2 nanowires (time span: 60 min). The plot also shows photocatalytic performance of P25-TiO_2 nanowires (0.08 g) in 50 ppm 100 ml solution in the same time span. (b) At different pH values 4, 7 and 11. (c) For different irradiation times i.e. 5 min, 15 min and 30 min.

The percentage of decolorization and photodegradation increases with increase in irradiation time. However, the reaction

rate decreases with irradiation time since it follows apparent first-order kinetics and additionally a competition for degradation may occur between the reactant and the intermediate products. In these studies we have used three different irradiation times: 5 min, 15 min and 30 min irradiation time as shown in Fig. 9c. The kinetics of degradation was found to be slower for 30 min irradiation time compared to 5 min and 15 min. This is attributed to the difficulty in converting the N-atoms of the dye into oxidized nitrogen compounds [50] and also to the slow reaction of short chain aliphatics with $OH^{\bullet}$ radicals [51].

4. Conclusions

We have presented here through systematic studies the performance of TiO_2 nanowires in sensing, quantification and photocatalytic degradation of cationic dyes in aqueous solution. Employment of TiO_2 for environmental concerns demonstrates yet another utility of the versatile TiO_2. Further improvements in titania nanowire morphology are necessary to improve sensitivity. Enhanced control of size and shape of titania nanowires can be achieved via additional optimization of polyol synthesis conditions (e.g. temperature), starting materials (e.g. (co-)solvents, titanium (-alkoxides) precursors [52,53]). Variation in surface chemical moieties (hydroxyl groups of the present study) would further allow detection of analytes of widely varying sizes and types. We envisage that requisite optimizations of the TiO_2 nanowires as proposed above will be beneficial for other applications (e.g. rechargeable lithium batteries).

Acknowledgements

The author thank I.S. Jarali (SSCU, IISc., Bangalore) for TGA, BET and FTIR measurements, Amit Mondal (INI, IISc., Bangalore) for TEM and Sumanta Mukherjee (SSCU, IISc.) for SEM.

Appendix A. Supplementary data

Supplementary data associated with this article can be found, in the online version, at doi:10.1016/j.talanta.2010.04.021.

References

[1] X. Chen, S.S. Mao, Chem. Rev. 107 (2007) 2891.
[2] F.E. Osterloh, Chem. Mater. 20 (2008) 35.
[3] D. Zhang, G. Li, X. Yang, J.C. Yu, Chem. Commun. (2009) 4381.
[4] A. Ghicov, P. Schmuki, Chem. Commun. (2009) 2791.
[5] Y. Wu, G. Lu, S. Li, J. Phys. Chem. 113 (2009) 9950.
[6] K. Shankar, J.I. Basham, N.K. Allam, O.K. Varghese, G.K. Mor, X. Feng, M. Paulose, J.A. Seabold, K.-S. Choi, C.A. Grimes, J. Phys. Chem. 113 (2009) 6327.
[7] D. Wang, Y. Liu, B. Yu, F. Zhou, W. Liu, Chem. Mater. 21 (2009) 1198.
[8] A.R. Armstrong, G. Armstrong, J. Canales, P.G. Bruce, Angew. Chem. Int. Ed. 43 (2004) 2286.
[9] (a) A. Manthiram, J. Kim, Chem. Mater. 10 (1998) 2895;
(b) S.K. Das, A.J. Bhattacharyya, J. Phys. Chem. C 113 (2009) 17367.
[10] S.J. Bao, Q.L. Bao, C.M. Li, Z.L. Dong, Electrochem. Commun. 9 (2007) 1233.
[11] M. Grätzel, Nature 44 (2001) 338.
[12] B. Tan, Y. Wu, J. Phys. Chem. B 110 (2006) 15932.
[13] M. Song, R. Zhang, X. Wang, Mater. Lett. 60 (2006) 2143.
[14] S. Liu, A. Chen, Langmuir 21 (2005) 8409.
[15] E. Topoglidis, C.J. Campbell, A.E.G. Cass, J.R. Durrant, Langmuir 17 (2001) 7899.
[16] G. Wang, Q. Wang, W. Lu, J. Li, J. Phys. Chem. B 110 (2006) 22029.
[17] L. Francioso, A.M. Taurino, A. Forleo, P. Siciliano, Sens. Actuators B 130 (2008) 70.
[18] N.E. Stankova, I.G. Dimitrov, T.R. Stoyanchov, P.A. Atanasov, Appl. Surf. Sci. 254 (2007) 1268.
[19] E. Formo, E. Lee, D. Campbell, Y. Xia, Nano Lett. 8 (2008) 668.
[20] S.O. Nielsen, D.J. Rose, A.S. Kubo, Science 185 (1974) 1183.
[21] C.D. Hollister, R. Anderson, G.R. Health, Science 213 (1981) 1321.
[22] J. Tong, Y. Chen, Environ. Sci. Technol. 41 (2008) 7126.
[23] M. Murakami, E. Imamura, H. Shinohara, K. Kiri, Y. Muramatsu, A. Harada, H. Takada, Environ. Sci. Technol. 42 (2008) 6566.
[24] M.L. Geagea, P. Stille, F.-G. Lafaye, M. Millet, Environ. Sci. Technol. 42 (2008) 692.
[25] http://dnr.wi.gov/wnrmag/html/supps/1999/aug99/threats.htm.
[26] A. Soares, B. Guieysse, B. Jefferson, E. Cartmell, J.N. Lester, Environ. Int. 34 (2008) 1033.
[27] M. Klavarioti, D. Mantzavinos, D. Kassinos, Environ. Int. 35 (2009) 227.
[28] P. Jiang, Z. Guo, Coord. Chem. Rev. 248 (2004) 205.
[29] H. Bayley, P.S. Cremer, Nature 413 (2001) 226.
[30] R. Métivier, I. Leray, B. Lebeau, B. Valeur, J. Mater. Chem. 15 (2005) 65.
[31] N.M. Mahmoodi, M. Arami, J. Photochem. Photobiol. B: Biol. 94 (2009) 20–24.
[32] K.V. Baiju, S. Shukla, S. Biju, M.L.P. Reddy, K.G.K. Warrier, Cat. Rep. 131 (2009) 663.
[33] H. Watanabe, T. Kunitake, Chem. Mater. 20 (2008) 4998.
[34] M.J. Jung, J.S. Im, K. Palnivelu, T. Kim, Y.S. Lee, J. Nanosci. Nanotechnol. 10 (2010) 297.
[35] J.-H. Chang, A.V. Ellis, Y.-H. Hsieh, C.-H. Tung, S.-Y. Shen, Sci. Total Environ. 407 (2009) 5914.
[36] X. Jiang, Y. Wang, T. Herricks, Y. Xia, J. Mater. Chem. 14 (2004) 695.
[37] R.A. Durst, A.J. Bäumner, R.W. Murray, R.P. Buck, C.P. Andrieux, Pure Appl. Chem. 69 (1997) 1317.
[38] M.G. Garguilo, N. Huynh, A. Proctor, A.C. Michael, Anal. Chem. 65 (1993) 523.
[39] Y. Liu, S. Wu, H. Ju, L. Xu, Electroanalysis 19 (2007) 986.
[40] X. Li, W. Zheng, L. Zhang, P. Yu, Y. Lin, L. Su, L. Mao, Anal. Chem. 81 (2009) 8557.
[41] M. Popa, M. Kakihana, Solid State Ionics 151 (2002) 251.
[42] (a) K. Nakamoto, Infrared and Raman Spectra of Inorganic Coordination Compounds, Wiley, New York, 1978, p. 220;
(b) D.C. Bradley, R.C. Mehrotra, D.P. Gaur, Metal Alkoxides, Academic Press, New York, 1978, p. 119;
(c) A.J. Maira, J.M. Coronado, V. Augugliaro, K.L. Yeung, J.C. Conesa, J. Soria, J. Catal. 202 (2001) 413.
[43] P. Kara, K. Kerman, D. Ozkan, B. Meric, A. Erdem, Z. Ozkan, M. Ozsoz, Electrochem. Commun. 4 (2002) 705.
[44] S.A. John, R. Ramaraj, Langmuir 12 (1996) 5689.
[45] M.A. Fox, M.T. Dulay, Chem. Rev. 93 (1993) 341.
[46] A.L. Linsebigler, G. Lu, J.T. Yates, Chem. Rev. 95 (1995) 735.
[47] I.K. Konstantinou, T.A. Albanis, Appl. Catal. B: Environ. 49 (2004) 1.
[48] I. Poulios, I. Tsachpinis, J. Chem. Technol. Biotechnol. 71 (1999) 349.
[49] S. Tunesi, M. Anderson, J. Phys. Chem. 95 (1991) 3399.
[50] J. Bandara, V. Nadtochenko, J. Kiwi, C. Pulgarin, Water Sci. Technol. 35 (1997) 87.
[51] C. Walling, Acc. Chem. Res. 8 (1975) 125.
[52] R.-C. Xie, J.K. Shang, J. Mater. Sci. 42 (2007) 6583.
[53] H.K. Yu, T.H. Eun, G.-R. Yi, S.-M. Yang, J. Colloid Interface Sci. 316 (2007) 175.